Interfacial polarization and pyroelectricity in antiferrodistortive structures induced by a flexoelectric effect and rotostriction

Anna N. Morozovska, Eugene A. Eliseev, Maya D. Glinchuk, Long-Qing Chen, and Venkatraman Gopalan

Phys. Rev. B **85**, 094107 — Published 21 March 2012

DOI: 10.1103/PhysRevB.85.094107

To be resubmitted to PRB

Interfacial Polarization and Pyroelectricity in Antiferrodistortive Structures Induced by a Flexoelectric Effect and Rotostriction

Anna N. Morozovska [1,2*], Eugene A. Eliseev[1], Maya D. Glinchuk[1], Long-Qing Chen[3], and Venkatraman Gopalan [3†]

[1] Institute for Problems of Materials Science, National Academy of Science of Ukraine, 3, Krjijanovskogo, 03142 Kiev, Ukraine

[2] Institute of Semiconductor Physics, National Academy of Science of Ukraine, 41, pr. Nauki, 03028 Kiev, Ukraine

[3]Department of Materials Science and Engineering, Pennsylvania State University, University Park, Pennsylvania 16802, USA

Abstract

Theoretical analysis based on the Landau-Ginzburg-Devonshire (LGD) theory is used to show that the combined effect of flexoelectricity and rotostriction can lead to a spontaneous polarization and pyroelectricity in the vicinity of antiphase boundaries, structural twin walls, surfaces and interfaces in the octahedrally tilted phase of otherwise non-ferroelectric perovskites such as $CaTiO_3$, $SrTiO_3$, and $EuTiO_3$. As an example, we numerically demonstrate a spontaneous polarization and pyroelectric response at the $SrTiO_3$ antiphase and twin boundaries at temperatures lower than the antiferrodistortive structural phase transition temperature of T_S~105 K in agreement with previously unexplained experimental results.

At temperatures lower than effective Curie temperature T_C^* (~25 K for twins and ~50 K for antiphase boundaries) biquadratic coupling between oxygen octahedron tilt and polarization vectors essentially enhances the polarization induced by the combined flexoelectric and rotostriction effects near the hard domain wall. Biquadratic coupling cannot induce polarization inside easy twins and antiphase boundaries, their polarization and pyroelectricity originates below T_S from the built-in flexoelectric field. The spontaneous polarization reaches the values ~0.1-5μC/cm^2 at the $SrTiO_3$ antiphase boundaries and twins without free charges. A principal difference between the influence of biquadratic and flexoelectric couplings on the interfacial polarization is the following: the biquadratic

* Corresponding author: morozo@i.com.ua

† Corresponding author: vxg8@psu.edu

coupling induces bistable ferroelectric polarization inside hard antiphase boundaries and hard twins below T_C^*, while the flexoelectric coupling induces improper spontaneous polarization via the flexoelectric field below T_S.

1. Introduction

Unique multifunctional properties of oxide interfaces are currently of widespread interest. These include such as 2-dimensional electron gas, superconductivity [1, 2, 3], charged domain walls [4], magnetism [5, 6] and multiferroicity at oxide interfaces [7] and thin strained films [8]. Interfaces by nature possess gradients of various order parameters such as strain, octahedral rotations, polarization, and magnetization, which can couple to induce new phenomena not present in the relevant bulk materials [9]. The influence of strain [10, 8] and strain gradients [11, 12, 13] in inducing ferroelectric polarization is well known. Recently, improper ferroelectricity induced by coupling to octahedral rotations has been predicted in a number of oxides (e.g. $YMnO_3$ [14], $Ca_3Mn_2O_7$ [15], $CaTiO_3$ [16]) and their multilayers [17].

Interfaces in antiferrodistorted perovskite oxides can possess both gradients in strain u_{ij} and in oxygen octahedral rotations, characterized by spontaneous octahedral tilt angles, which in turn can be described by an axial vector Φ_i (i=1, 2, 3) [18]. As a consequence, both direct flexoelectric effect, namely the creation of a ferroelectric polarization due to a strain gradient, as well as rotostriction, namely a quadratic coupling between octahedral rotations and strain, exist at such interfaces. The coupling between these two phenomena can thus lead to a ferroelectric polarization at an interface across which the octahedral rotation varies, which is the subject of this paper. It has been previously predicted that a spontaneous polarization vector P_i can appear inside structural walls due to biquadratic coupling term $\eta_{ijkl} P_i P_j \Phi_k \Phi_l$ [19, 20], but it is absent in the bulk. The biquadratic coupling term was later regarded as Houchmandazeh-Laizerowicz-Salje (HLS) coupling [21]. The coupling was considered as the reason of magnetization appearance inside the ferromagnetic domain wall in non-ferromagnetic media [22]. Biquadratic coupling leads to a polarization appearance inside antiphase boundaries in $SrTiO_3$ below 50 K [20]. Zubko et al [23] experimentally observed strong changes of the apparent flexoelectric coefficient in $SrTiO_3$ at much higher temperatures, namely below the antiferrodistortive structural phase transition temperature (105 K), and supposed one of its possible reasons in the polarization appearance at the domain walls between twins. Recently Salje et al directly observed ferrielectric polarization at ferroelastic domain boundaries in $CaTiO_3$ by aberration-corrected Transmission Electron Microscopy (TEM) at room temperature [24].

To the best of our knowledge, the flexoelectricity-induced polarization appearance across the structural twin boundaries (**TB**), antiphase boundaries (**APB**) and interfaces has not been previously addressed. However, the flexoelectric coupling, which is nonzero in any material and strong enough in many perovskites [11, 13, 23, 25, 26, 27, 28], should lead to the spontaneous polarization appearance across the structural domains walls of otherwise non-ferroelectric perovskites. Direct gradient coupling between the order parameters could lead to the oscillatory solutions and non-uniform pattern formation [29, 30]. This motivates us to perform calculations, based on the LGD free energy, to study the impact of flexoelectric coupling on the spontaneous polarization in the vicinity of structural domain walls in non-ferroelectric tilted perovskites such as $SrTiO_3$, $CaTiO_3$, and $EuTiO_3$. We present results for 90-degree TB and 180-degree APB in bulk $SrTiO_3$.

2. Theoretical formalism

Following Tagantsev et al [20], we analyze the domain wall energy using approximate free energy functional corresponding to Tailor expansion on the polar and structural order parameter components. In the parent high temperature phase above the structural phase transition, the free energy density has the form:

$$\begin{aligned} F_b = {} & a_i(T)P_i^2 + a_{ij}^u P_i^2 P_j^2 + \ldots + \frac{g_{ijkl}}{2}\left(\frac{\partial P_i}{\partial x_j}\frac{\partial P_k}{\partial x_l}\right) - P_i\left(\frac{E_i^d}{2} + E_i^{ext}\right) - q_{ijkl}u_{ij}P_k P_l + \frac{c_{ijkl}}{2}u_{ij}u_{kl} \\ & + b_i(T)\Phi_i^2 + b_{ij}^u\Phi_i^2\Phi_j^2 - \eta_{ijkl}^u P_i P_j \Phi_k\Phi_l + \frac{v_{ijkl}}{2}\left(\frac{\partial \Phi_i}{\partial x_j}\frac{\partial \Phi_k}{\partial x_l}\right) \\ & - r_{ijkl}^{(\Phi)}u_{ij}\Phi_k\Phi_l + \frac{f_{ijkl}}{2}\left(\frac{\partial P_k}{\partial x_l}u_{ij} - P_k\frac{\partial u_{ij}}{\partial x_l}\right) - \Phi_i\tau_i^d \end{aligned} \quad (1)$$

Φ_i is the components (i=1, 2, 3) of an axial **tilt vector** corresponding to the octahedral rotation angles [18] (see **Fig. 1**), τ_i^d is de-elastification torque [18]; $u_{ij}(\mathbf{x})$ is the strain tensor. The summation is performed over all repeated indices. Coefficients $a_i(T)$ and $b_i(T)$ temperature dependence can be fitted with Barrett law for quantum paraelectrics [31]: $a_1(T) = \alpha_T T_q^{(E)}\left(\coth\left(T_q^{(E)}/T\right) - \coth\left(T_q^{(E)}/T_0^{(E)}\right)\right)$ and $b_1(T) = \beta_T T_q^{(\Phi)}\left(\coth\left(T_q^{(\Phi)}/T\right) - \coth\left(T_q^{(\Phi)}/T_S\right)\right)$. Gradients coefficients g_{ij} and v_{ij} are regarded positive for commensurate ferroics. f_{ijkl} is the forth-rank tensor of flexoelectric coupling, q_{ijkl} is the forth-rank electrostriction tensor, $r_{ijkl}^{(\Phi)}$ is the rotostriction tensor. The biquadratic coupling between Φ_i and polarization components P_i are defined by the constants η_{ijkl}. The flexoelectric effect tensor f_{ijkl} and

rotostriction tensor $r_{ijkl}^{(\Phi)}$ have nonzero components in all phases and for any symmetry of the system. Tensors form for cubic *m3m* symmetry is well-known; in particular f_{12}, f_{11} and f_{44} are nonzero [23] similarly to elastic constants and electrostriction tensors [32]. Note, that the inclusion of the flexoelectric Lifshitz term in the free energy is critical for all effects discussed below.

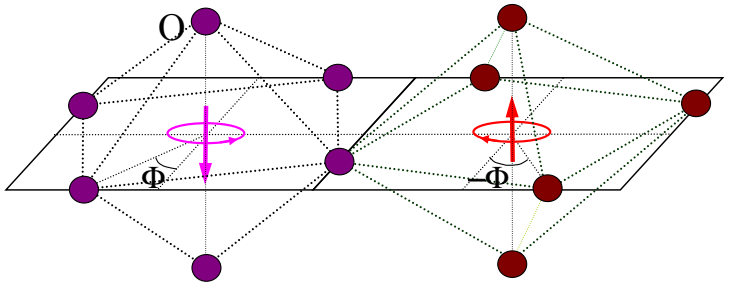

Figure 1. The tilt value is typically opposite for the neighboring oxygen octahedrons far from the domain boundaries [18]. For the case free energy (1) considers the quasi-continuum tilt behavior in the next-nearest octahedral [20, 30].

External field is E_i^{ext}. In general case polarization distribution $P_i(x_i)$ can induce the depolarization field E_i^d inside the wall. In the dielectric limit E_i^d obeys electrostatic equation:

$$\varepsilon_0\varepsilon_b \frac{\partial E_i^d}{\partial x_i} = -\frac{\partial P_i}{\partial x_i}, \qquad (i=1, 2, 3) \tag{2}$$

where $\varepsilon_0=8.85\times10^{-12}$ F/m is the universal dielectric constant, ε_b is the "base" isotropic lattice permittivity, different from the ferroelectric soft mode permittivity [33, 34, 35, 36]. Semiconductor case is considered elsewhere [37].

Euler-Lagrange equations of state are obtained from the minimization of the free energy (1) as

$$\frac{\partial F_b}{\partial \Phi_i} - \frac{\partial}{\partial x_j}\left(\frac{\partial F_b}{\partial(\partial\Phi_i/\partial x_j)}\right) = 0, \quad \frac{\partial F_b}{\partial P_i} - \frac{\partial}{\partial x_j}\left(\frac{\partial F_b}{\partial(\partial P_i/\partial x_j)}\right) = 0 \quad \frac{\partial F_b}{\partial u_{ij}} - \frac{\partial}{\partial x_k}\left(\frac{\partial F_b}{\partial(\partial u_{ij}/\partial x_k)}\right) = \sigma_{ij} \tag{3}$$

Where $\sigma_{ij}(\mathbf{x})$ is the stress tensor that satisfies mechanical equilibrium equation $\partial\sigma_{ij}(\mathbf{x})/\partial x_j = 0$. Note, that the stress tensor, polarization and tilt gradients vanish far from the domain walls.

Equation of state (3c) could be rewritten via the strains $u_{ij}(\mathbf{x})$ as follows:

$$u_{mn} = s_{mnij}\sigma_{ij} + R_{mnkl}^{(\Phi)}\Phi_k\Phi_l + Q_{mnkl}P_k P_l - F_{mnkl}\frac{\partial P_k}{\partial x_l}. \tag{4}$$

Where s_{mnij} is the elastic compliances tensor; $R_{ijkl}^{(\Phi)} = s_{ijmn} r_{mnkl}^{(\Phi)}$ is the rotostriction strain tensor; $Q_{ijkl} = s_{ijmn} q_{mnkl}$ is the electrostriction strain tensor; $F_{ijkl} = s_{ijmn} f_{mnkl}$ is the flexoelectric strain tensor. The latter term corresponds to inverse flexoelectric effect.

The inhomogeneous strain $u_{ij}(\mathbf{x})$ given by Eq.(4) induces the polarization variation $\delta P_i(\mathbf{x})$ across the structural APB and TB, domain walls, defects and interfaces due to the direct flexoelectric effect:

$$\delta P_i(\mathbf{x}) \sim a_{iv}^{-1} f_{mnvl} \frac{\partial u_{mn}}{\partial x_l} \sim - a_{iv}^{-1} f_{mnvl} R_{mnpq}^{(\Phi)} \frac{\partial(\Phi_p \Phi_q)}{\partial x_l}. \quad (5)$$

The term $f_{mnvl} \frac{\partial u_{mn}}{\partial x_l}$ denotes direct flexoelectric effect. Note, that Eq.(5) is valid only for zero electric field, including both external and depolarization fields. The proportionality in Eq.(5) suggests that the product of the flexoelectric f_{mnvl} and rotostriction $R_{mnpq}^{(\Phi)}$ coefficients leads to the appearance of spontaneous polarization, which will *be abbreviated* in this study as **flexo-roto-effect**. To the best of our knowledge, the flexoelectric contribution to the interfacial polarization has not been considered earlier.

The gradient in the octahedral tilts across APB or TB may lead to a rather strong interfacial polarization due to the derivatives of the rotation angle in Eq.(5). In the next section we will consider the concrete example of $SrTiO_3$ with known numerical values of $R_{mnkj}^{(\Phi)}$ and F_{mnvl} to check the validity of this supposition.

3. Flexo-roto-effect contribution to the interfacial polarization and pyroelectricity

Below we consider several one-dimensional problems, which follow from general results of the previous section, namely a typical 180-degree APB and 90-degree TB. Stable solutions of the coupled Euler-Lagrange equations (3) were obtained numerically by iteration method. We set initial distributions of the tilt and polarization vectors, which satisfy the boundary conditions. Special attention was paid to the parity of the obtained polarization distributions, namely we consider both odd and even initial polarization distributions with respect to the domain wall plane. Iterations were stopped when the relative tolerance reaches the value 10^{-4}.

Note, that Tagantsev et al [20] obtained nonzero polarization across APB in $SrTiO_3$ below $T_C^* \sim 40$ K, where T_C^* is a local ferroelectric transition temperature in APB in a free crystal. The flexoelectric coupling was not included into the calculations performed in Ref.[20], while mentioned in

the paper as giving rise to the renormalization of the gradient terms. One of the most important results we obtained in the present research is the fact that the flexoelectric effect primary leads to the appearance of the strong built-in electric fields across the wall, besides the renormalization of the polarization gradient term also considered in Ref.[27]. We obtained that the flexoelectric effect can induce the polarization and pyroelectric response across TB and APB walls over the entire temperature range of the structural phase T_S<105 K.

Despite odd distributions seems to be more energetically preferable [37], one may ask a question about the experimental observation of odd polarization and pyroelectric response distributions across an interface, because the mean values are zero in this case. Using aberration-corrected TEM combined with atomic column shape image analysis (proposed earlier in Ref.[38]) it is possible to achieve **picometer** resolution (0.025 nm for atomic coordinates) and do observe spontaneous polarization at ferroelastic domain twin boundaries [24]. To the best of our understanding, Figures 2e-f in Ref.[24] reliably demonstrate signatures of both even and odd polarization distributions across ferroelastic twins in $CaTiO_3$. So we hope that local spontaneous polarization of elastic domain walls in ferroelastics like $CaTiO_3$, $SrTiO_3$, and $EuTiO_3$ can be reliably observed by aberration-corrected TEM.

Below we show that all ferroelastic domain walls possess noticeable pyroelectric coefficient that can be of odd and even-type with respect to the domain wall plane. Spatial distribution of pyroelectric coefficient (regarded as local pyroelectric response) can be directly measured by the novel scanning probe pyroelectric microscopy (PyroSPM), where the resolution limit 50 nm was already achieved [39]. Similar to the conventional piezoelectric force microscopy, where the lateral resolution is at least 2-5 times smaller the tip effective size (see e.g. Fig.12 in Ref.[40]), the resolution in PyroSPM is primarily determined by the sharpness of the tip. So, scanning with tips of sizes 5-10 nm [41] allow registration of local piezoresponse and with lateral resolution ~2-5 nm (see e.g. Ref.[41, 42], and refs therein) and potentially local pyroelectric response with the same resolution. Since halfwidth of "hard" APB and TB in $SrTiO_3$ is about 3-5 nm [20, 37], PyroSPM could reliably detect pyroelectric response averaged over the wall width. Thus below we consider the influence of the flexoelectric and rotostriction effect on both odd and even polarization distributions across TB and APB. Also we calculate maximal values of pyroelectric coefficient as well as average the values over domain the walls width.

3.1. Flexo-roto-effect manifestation at the antiphase boundaries (APB)

In the octahedral tilted phase at $T < T_S$, the one-component spontaneous tilt, Φ_3^S, appear in a bulk $SrTiO_3$, other components, Φ_1 and Φ_2, can be nonzero in the vicinity of APB. "Easy" APB with $\Phi_3(x_3) \neq 0, \Phi_2 \equiv 0, \Phi_1 \equiv 0$ (see **Fig. 2a**) induces nonzero odd or even distribution of polarization $P_3(x_3)$, while $P_1 \equiv 0$, $P_2 \equiv 0$. "Hard" APB with $\Phi_1(x_1) \neq 0$, $\Phi_3(x_1) \neq 0$, $\Phi_2 \equiv 0$ (see **Fig. 2b**) induces nonzero odd or even distributions of polarization $P_1(x_1)$ and even distribution of $P_3(x_1)$, while $P_2 \equiv 0$. Classification "easy" and "hard" APB comes from Ref.[20].

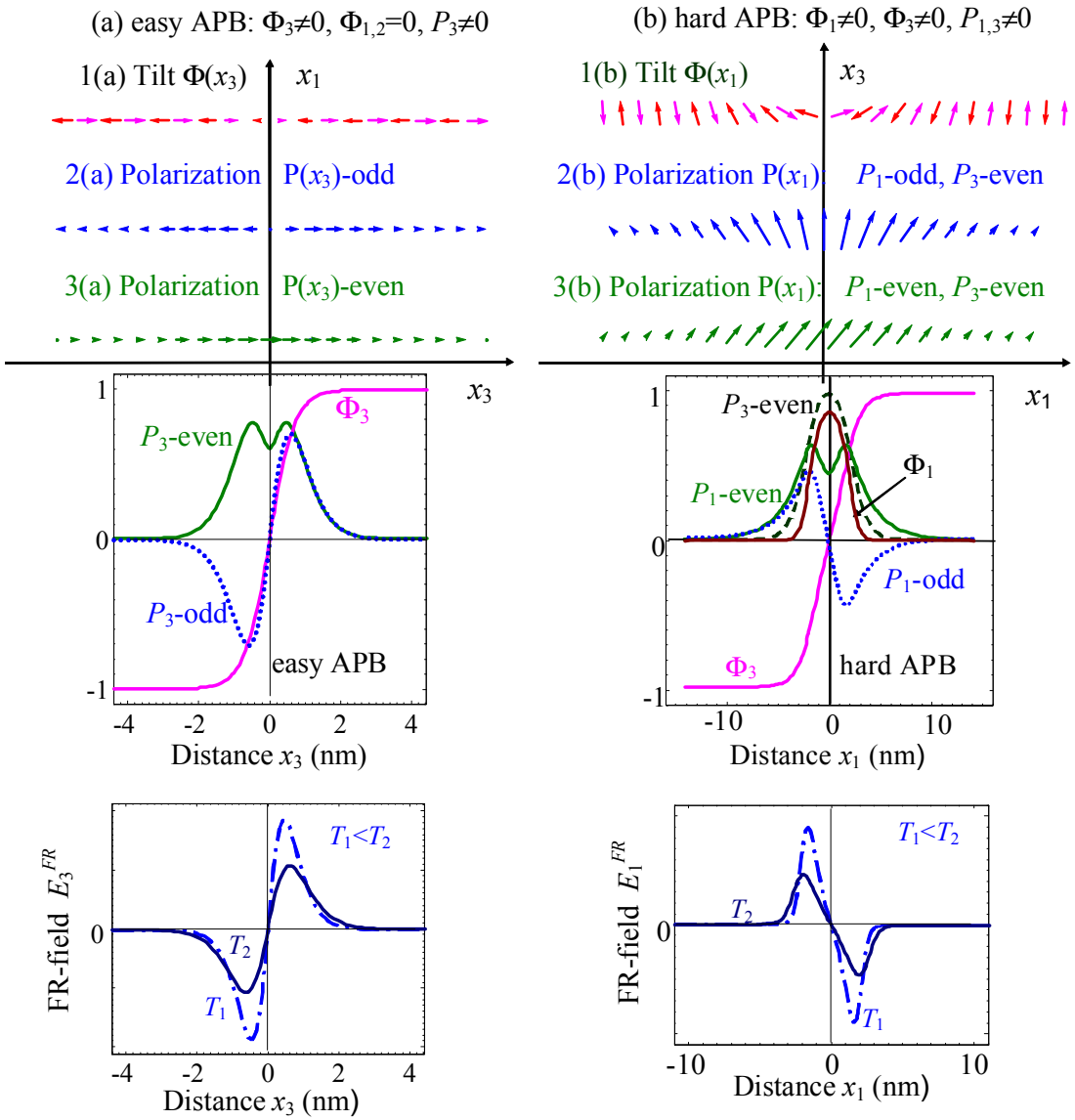

Figure 2. Schematics of the polarization appearance inside easy (a) and hard (b) APB. x_1=[100], x_3=[001] and x_2=[010] (not shown), are crystallographic axes directions of $SrTiO_3$. Flexo-roto field,

which induces the polarization component parallel to the wall, is shown at the bottom plots at two different temperatures $T_1 < T_2$. Note, that Vasudevarao et al [8] observed and calculated by phase-field various orientations of the ferroelestic APB in $SrTiO_3$.

For the case of **hard APB** (x_1-dependent solution) we derive the stress field and simplify the evident form of Eqs.(3) as listed in the section **S1**, **Suppl.Mat [43]**. Distributions $\Phi_{1.,3}(x_3)$ and $P_{1.,3}(x_3)$ are shown schematically in **Fig. 2b** (right). Appeared that $\Phi_{1.,3}(x_3)$ are rather weakly dependent on the polarization vector. Nonzero odd electric field $E_1^{FR} = -F_{12}(s_{11}+s_{12})^{-1}\partial\left(\left(R_{11}^{(\Phi)}+R_{12}^{(\Phi)}\right)\Phi_3^2 + 2R_{12}^{(\Phi)}\Phi_1^2\right)/\partial x_1$ induced by flexoelectric effect and rotostriction (abbreviated as **flexo-roto field** below) exists only for the polarization component $P_1(x_1)$ perpendicular to APB plane (see bottom **Fig.2b**). It is clear that the odd field makes odd-type distribution of $P_1(x_1)$ favourable. The component P_1 appears just below T_S and strongly depends on the tilt vector as proportional to the field E_1^{FR}. Hysteresis loop for polarization component P_1 is absent in external field E_1^{ext} due to the strong depolarization field $E_1^d(x_1) = -P_1(x_1)/(\varepsilon_0\varepsilon_b)$. Nonzero component P_1 perpendicular to the APB should induce the component P_3 parallel to the APB just below T_S due to the biquadratic coupling term $-\eta_{44}\Phi_1\Phi_3P_1$. Thus the trivial solution $P_1 \equiv P_3 \equiv 0$ does not exist in the vicinity of hard APB due to nonzero odd $E_1^{FR} \neq 0$ and the coupling term $-\eta_{44}\Phi_1\Phi_3P_1$ (compare with Ref.[20], where the stability of the trivial solution $P_3 \equiv 0$ was studied without flexo-effect). The effective Curie temperature $T_C^{APB} \approx 50$ K can be introduced for hard APB. Ferroelectric hysteresis for polarization component $P_3(E_3^{ext})$ should exist in the temperature range $T < T_C^{APB}$. Below T_C^{APB} the perpendicular component P_1 is induced by the sum of the coupling term $-\eta_{44}\Phi_1\Phi_3P_3$ and flexo-roto field E_3^{FR}. The depolarization field strongly reduces the component P_1 in comparison with ferroelectric polarization P_3 below T_C^{APB}. Pyroelectric coefficients $\Pi_3 = dP_3/dT$ and $\Pi_1 = dP_1/dT$ are nonzero in the temperature range $T < T_S$, but their temperature behavior are rather different at $T_C^{APB} < T < T_S$ and $T < T_C^{APB}$ as shown in **Figs. 3**.

Under the absence of the flexoelectric field the spontaneous polarization and pyroelectric coefficient are zero at temperatures higher than the effective Curie temperature T_C^{APB} (see curves 1,2 calculated at $F_{ij} \equiv 0$ and $\eta_{ij} \neq 0$ in **Figs. 3**). The flexoelectric field rather weakly influences on the

polarization component P_3 (compare curves 1, 2 with curves 3, 4 in **Fig.3a**). However the flexoelectric field E_1^{FR} strongly increases the component P_1 below T_S, since $P_1 \sim E_1^{FR}$ (compare curves 1, 2 with curves 3, 4 in **Fig.3b**). Actually, for the case $F_{ij} \neq 0$ the component P_1 appears below T_S, firstly quasi-linearly increases with temperature decrease, then has a pronounced jump at T_C^{APB} and then saturates at temperatures $T << T_q$. The break at T_C^{APB} originates from the appearance of reversible polarization component P_3 below T_C^{APB}. The component $P_1 \sim E_1^{FR} \sim \dfrac{\partial \Phi^2}{\partial x_1} \sim \left(\Phi_3^S\right)^2 / l_\Phi \sim \left(-b_1(T)\right)^{3/2} \sim \left(T_S - T\right)^{3/2}$ in the vicinity of T_S, where $l_\Phi = \sqrt{-v_{11}/b_1(T)}$ is the correlation length. Note, that Tagantsev et al [20] analytically predicted spontaneous polarization about 4 μC/cm^2 at hard APB below 35-40 K without considering flexo-roto-effect contribution. Allowing for the flexo-roto-effect we obtained P_3~8 μC/cm^2 and P_1~0.1 μC/cm^2 at hard APB below T_C^{APB}≈50 K. At temperatures $T < T_C^{APB}$ the amplitude of P_1 is much smaller than the amplitude of P_3 due to the strong depolarization field $E_1^d(x_1)$.

It is seen from the **Figs. 3c-d** that pyroelectric coefficients Π_3 and Π_1 appears below $T_S = 105$K only at nonzero flexoelectric coefficient $F_{12} \neq 0$. Pyroelectric coefficient Π_3 has the sharp maximum at T_C^{APB} corresponding to the second order ferroelectric phase transition (appearance of the ferroelectric polarization P_3). Pyroelectric coefficient Π_1 has two maximums: a smooth maximum at the polarization inflection point ~80 K and the sharp maximum at T_C^{APB} originated from P_3 appearance, since P_3 enhances P_1 via the biquadratic coupling term $-\eta_{44}\Phi_1\Phi_3 P_3$. Pyroelectric coefficients monotonically decrease below T_C^{APB} with the temperatures decrease due to the spontaneous polarization components saturation at temperatures $T << T_q$. Actually, in the range $T << T_q$ polarization becomes almost temperature independent and its temperature derivative vanishes.

Allowing for the flexo-roto-effect contribution we calculated noticeable pyroelectric coefficients of the even-type distributions *averaged across hard APB*: $\langle\Pi_3\rangle$~2×10^{-3} C/m^{2}K around T_C^{APB} and $\langle\Pi_1\rangle$~1×10^{-5}C/m^{2}K. The values are well above detectable limits of pyroelectric coefficient, which are about (10^{-6}–10^{-7})C/m^{2}K [44]. The halfwidth of hard APB is not less than 3 nm at 0 K and 5 nm at 90 K (see **Fig.S2, Suppl.Mat. [43]**) Thus PyroSPM [39] supplied with sharp tips of sizes 5-10 nm could reliably detect pyroelectric response averaged over the APBs width.

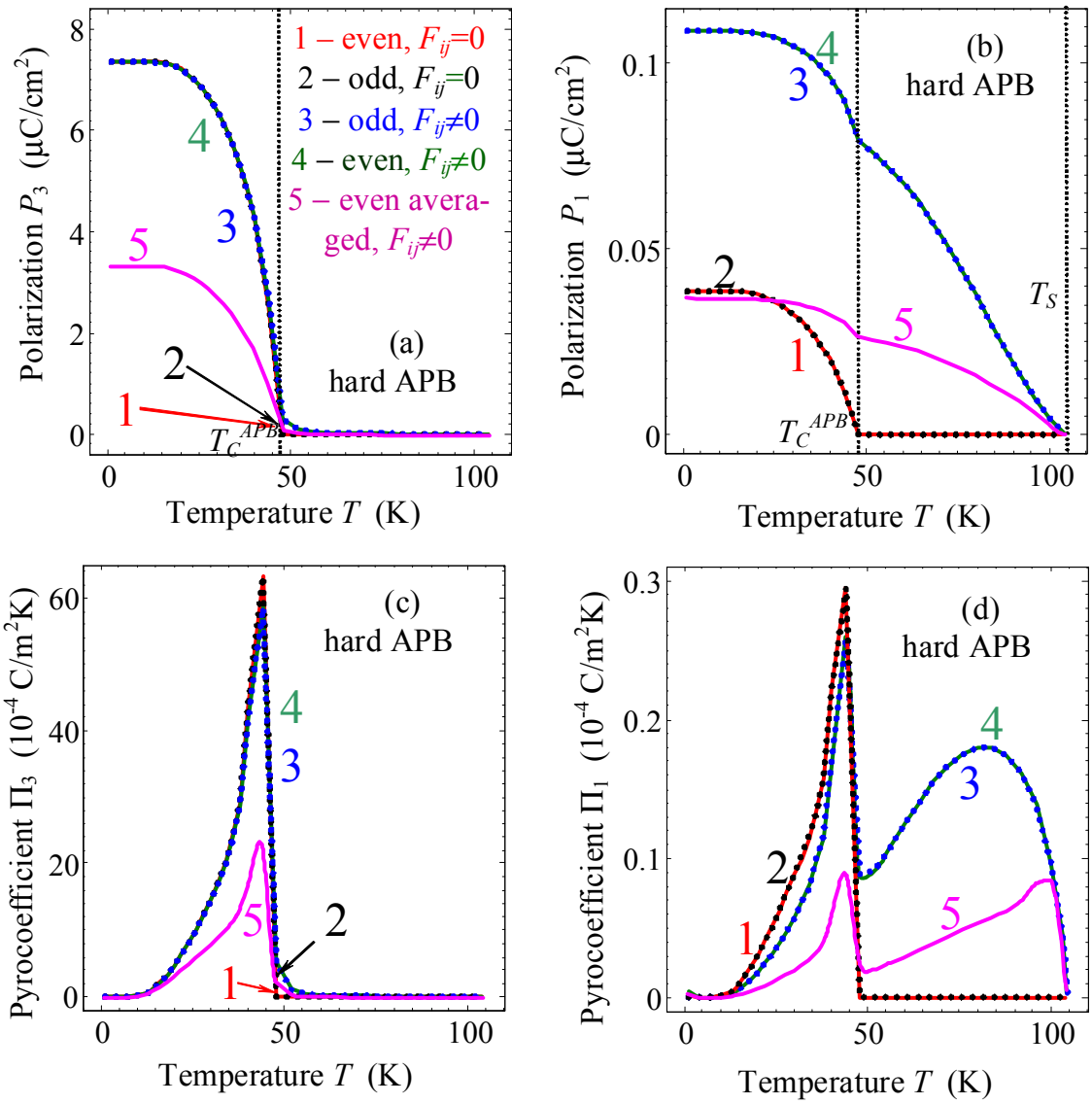

Figure 3. Temperature dependences of spontaneous polarization components P_3 and P_1 (a,b) and corresponding pyro-coefficient components Π_3 and Π_1 values (c,d) calculated for hard APB in $SrTiO_3$ without free screening charges. Temperature dependences are calculated for nonzero flexoelectric effect $F_{ij} \neq 0$ and biquadratic coupling $\eta_{ij} \neq 0$ (curves 3, 4, 5) and for the case of nonzero biquadratic coupling $\eta_{ij} \neq 0$ and zero flexoelectric effect $F_{ij} \equiv 0$ (curves 1, 2). Curves 1-4 are maximal values, curves 5 – are the even-type distributions *averaged across APB width,* which temperature dependence is shown in **Fig.S2, Suppl. Mat [43]**. Curves 1-5 style and colour coding for plots (a-d) are the same and described in the legend to plot (a). Solid and dotted curves correspond to P_3-even and P_3-odd solutions respectively. Material parameters are listed in the **Table 1.**

Table 1. $SrTiO_3$ material parameters and LGD free energy (1) coefficients collected from Refs. [20, 23, 31, 45, 46, 47, 48, 49]

Parameter	SI units	Value	Source and notes
ε_b	dimensionless	43	[48]
α_T	$10^6\times$m/(F K)	0.75	[20, 46]
$T_0^{(E)}$	K	30	ibidem
$T_q^{(E)}$	K	54	ibidem
a_{ij}	$10^9\times$m^5/(C^{2}F)	a_{11}^u=2.025, a_{12}^u=1.215, a_{11}^σ=0.820, a_{12}^σ=1.396	ibidem
q_{ij}	$10^{10}\times$ m/F	q_{11}=1.251, q_{12}= –0.108, q_{44}=0.243	[46]
Q_{ijkl}	m^4/C^2	Q_{11}=0.051, Q_{12}= –0.016, Q_{44}=0.020	[20]
g_{ijkl}	$10^{-11}\times$V·m^3/C	g_{11}=g_{44}=1, g_{12}=0.5	Estimation [49]
β_T	$10^{26}\times$J/(m^5 K)	9.1	[46]
T_S	K	105	[46]
$T_q^{(\Phi)}$	K	145	[46]
b_{ij}	$10^{50}\times$J/m^7	b_{11}^u=1.94, b_{12}^u=3.96, b_{11}^σ=0.93, b_{12}^σ=3.88	[46]
r_{ij}	$10^{30}\times$J/(m^5)	r_{11}=1.3, r_{12}= –2.5, r_{44}=-2.3	[46]
R_{ij}	$10^{19}\times$m^{-2}	R_{11}=0.882, R_{12}= –0.777, R_{44}= –1.811	calculated from r
η_{ijkl}	10^{29} (F m)$^{-1}$	η_{11}^u=-3.366, η_{12}^u= 0.135, η_{44}^u=6.3 η_{11}^σ=-2.095, η_{12}^σ= –0.849, η_{44}^σ=5.860	[46] calculated from η_{ij}^u
v_{ijkl}	$10^{10}\times$J/m^3	v_{11}=0.28, v_{12}= –7.34, v_{44}=7.11	[20]
c_{ij}	$10^{11}\times$J/m^3	c_{11}=3.36, c_{12}=1.07, c_{44}=1.27	[20, 46]
s_{ij}	$10^{-12}\times$m^3/J	s_{11}=3.52, s_{12}= –0.85, s_{44}=7.87	calculated from c_{ij}
F_{ijkl}	$10^{-12}\times$m^3/C	F_{11}= – 13.80, F_{12}= 6.66, F_{44}= 8.48	calculated from f_{ij} from [23] at given stress
Φ_S	radian	0.0235	at low temperatures
n_e	m^{-3}	$10^{22} - 5\cdot10^{26}$	[50, 51], strongly dependent on the oxygen vacancies concentration

***)** Superscripts "u" and "σ" denote coefficients at given strain (clamped sample) and given stress (free sample) respectively

For the case of **easy APB** (x_3-dependent solution) one could easily derive the stress field and the evident form of Eqs.(3) as listed in the section **S2**, **Suppl.Mat [43].** Distributions of $\Phi_3(x_3)$ and $P_3(x_3)$ are shown schematically in **Fig. 2a** (right). The tilt $\Phi_3(x_3)$ profile is rather weakly dependent on the polarization vector distribution and could be well approximated as $\Phi_3 = \Phi_3^S \tanh\left(x_3 / \sqrt{2} l_\Phi\right)$. In contrast, polarization P_3 strongly depends on the tilt vector as proportional to the odd flexo-roto field $E_3^{FR} = -2F_{12}R_{12}^{(\Phi)}\left(s_{11}+s_{12}\right)^{-1}\partial\left(\Phi_3^2\right)/\partial x_3$ (see bottom **Fig.2a**). The trivial solution $P_3 \equiv 0$ does not exist

in the vicinity of APB due to nonzero flexo-roto field $E_3^{FR} \neq 0$. So the spontaneous polarization component P_3 perpendicular to the APB plane is induced by the flexo-roto-field E_3^{FR} only. The depolarization field $E_3^d(x_3) = -P_3(x_3)/(\varepsilon_0 \varepsilon_b)$ [52] strongly reduces P_3 value. The "true" ferroelectricity, i.e. polarization hysteresis is absent in external field E_3^{ext}, but nonzero pyroelectric response $\Pi_3 = dP_3/dT$, should exist, since the polarization component is temperature dependent [37]. We omit quantitative analyses of the results for the easy APB in $SrTiO_3$, because their halfwidth $\sim l_\Phi(T) = \sqrt{-v_{11}/b_1(T)}$ appeared not more than 1 nm for temperatures less that 90 K (see **Fig. S2** in **Suppl.Mat. [43]**), at that sometimes the distance between polarization maxima and minima is less than the unit cell at T<90 K. The features scale less than 1 nm is well beyond applicability of the continuous medium theory we used in the paper.

3.2. Flexo-roto-effect manifestation at 90-degree TB

90-degree twins can have structure with rotation vector parallel (**Fig.4a**) or perpendicular (**Fig.4b**) to the domain wall plane in the immediate vicinity of the plane. Far from the wall the tilt vectors of twins are perpendicular. We will regard parallel twins as "**hard**" TB, since they have higher energy and perpendicular twins as "**easy**" TB, since they have lower energy as demonstrated in the section **S4, Suppl. Mat [43].** The evident form of Eqs.(3) for twins are listed in the section **S3**, **Suppl.Mat [43].**

The flexo-roto field $\widetilde{E}_1^{FR}(\widetilde{x}_1)$ exist for 90-degree twins; it is an odd function with more complex structure than the one for APBs, (see bottom **Figs.4a** and **4b** and compare them with the bottom **Figs.2a** and **2b**). Polarization hysteresis for $\widetilde{P}_1(\widetilde{E}_1^{ext})$ component is absent in the dielectric limit due to the strong depolarization field $\widetilde{E}_1^d(\widetilde{x}_1) = -\widetilde{P}_1(\widetilde{x}_1)/(\varepsilon_0 \varepsilon_b)$. Nonzero component $\widetilde{P}_1$ perpendicular to the TB induces the component $\widetilde{P}_2$ parallel to the TB just below T_S due to the biquadratic coupling term $-\widetilde{\eta}_{66}\widetilde{\Phi}_1\widetilde{\Phi}_2\widetilde{P}_1$. The trivial solution $\widetilde{P}_1 \equiv \widetilde{P}_2 \equiv 0$ does not exist in the vicinity of hard TB due to nonzero flexo-roto field $\widetilde{E}_1^{FR} \neq 0$ and the coupling term $-\widetilde{\eta}_{66}\widetilde{\Phi}_1\widetilde{\Phi}_2\widetilde{P}_1$. Due to the biquadratic coupling terms $-\widetilde{\eta}_{11}\widetilde{\Phi}_2^2 - \widetilde{\eta}_{12}\widetilde{\Phi}_1^2$ and elastic fields polarization component $\widetilde{P}_2$ depends on the tilt vector and becomes ferroelectric at temperatures $T < T_C^{TB}$, where the effective Curie temperature $T_C^{TB} \approx 20$ K exists for hard twins in $SrTiO_3$. Therefore ferroelectric hysteresis for polarization component $\widetilde{P}_2(\widetilde{E}_2^{ext})$ should exist in

the temperature range $T < T_C^{TB}$. Via the biquadratic coupling term $\widetilde{\eta}_{66}\widetilde{\Phi}_2\widetilde{\Phi}_1\widetilde{P}_2$ the ferroelectric parallel component $\widetilde{P}_2$ strongly enhances the perpendicular component $\widetilde{P}_1\left(\widetilde{E}_1^{FR}\right) \sim \widetilde{E}_1^{FR}$ below T_C^{TB}. Pyroelectric coefficients $\widetilde{\Pi}_2 = d\widetilde{P}_2 \big/ dT$ and $\widetilde{\Pi}_1 = d\widetilde{P}_1 \big/ dT$ should be nonzero in the temperature range $T < T_S$ as shown below.

Under the absence of the flexo-roto field $\widetilde{E}_1^{FR}$ spontaneous polarization and pyroelectric coefficient are zero inside **easy TB**. Their spontaneous polarization component appears below $T_S = 105$ K at $F_{12} \neq 0$, then quasi-linearly increases with temperature decrease and then saturates at temperatures $T < T_0^{(E)} \sim 30$ K. Actually, $\widetilde{P}_1 \sim \widetilde{E}_1^{FR} \sim \partial\left(\Phi_2^2\right) \big/ \partial \widetilde{x}_1 \sim \left(\Phi_S\right)^2 \big/ l_\Phi \sim \left(-b_1(T)\right)^{3/2} \sim \left(T_S - T\right)^{3/2}$ at temperatures near T_S. Pyroelectric coefficient Π_3 appears below $T_S = 105$ K at $F_{12} \neq 0$ [37]. Below we omit quantitative analyses of the results for the easy TB in $SrTiO_3$, because their halfwidth appeared not more than 1 nm for temperatures less that 90 K (see **Fig. S2** in **Suppl.Mat. [43]**), at that sometimes the distance between polarization maxima and minima is less than the unit cell. As we argued for easy APB, the features scale less than 1 nm cannot be described quantitatively the continuous medium theory. Note, that easy TB halfwidth noticeably increases with temperature increase only at *T*>90 K, while polarization amplitude strongly decreases with temperature increase above 90 K and disappears at 105 K.

Polarization and pyroelectric coefficient spatial distribution across hard TB and its temperature behavior are qualitatively similar to the ones calculated for hard APB. However, numerical values of polarization and pyroelectric coefficient for hard TBs are typically smaller than for hard APBs (compare **Figs. 3** with **Figs. 5**). The difference originated from the smaller effective flexoelectric field, which in turn originate from smaller stress gradients. Differences in the stress gradients originate from the different orientation of the tilt vector **Φ** inside hard TB and APB.

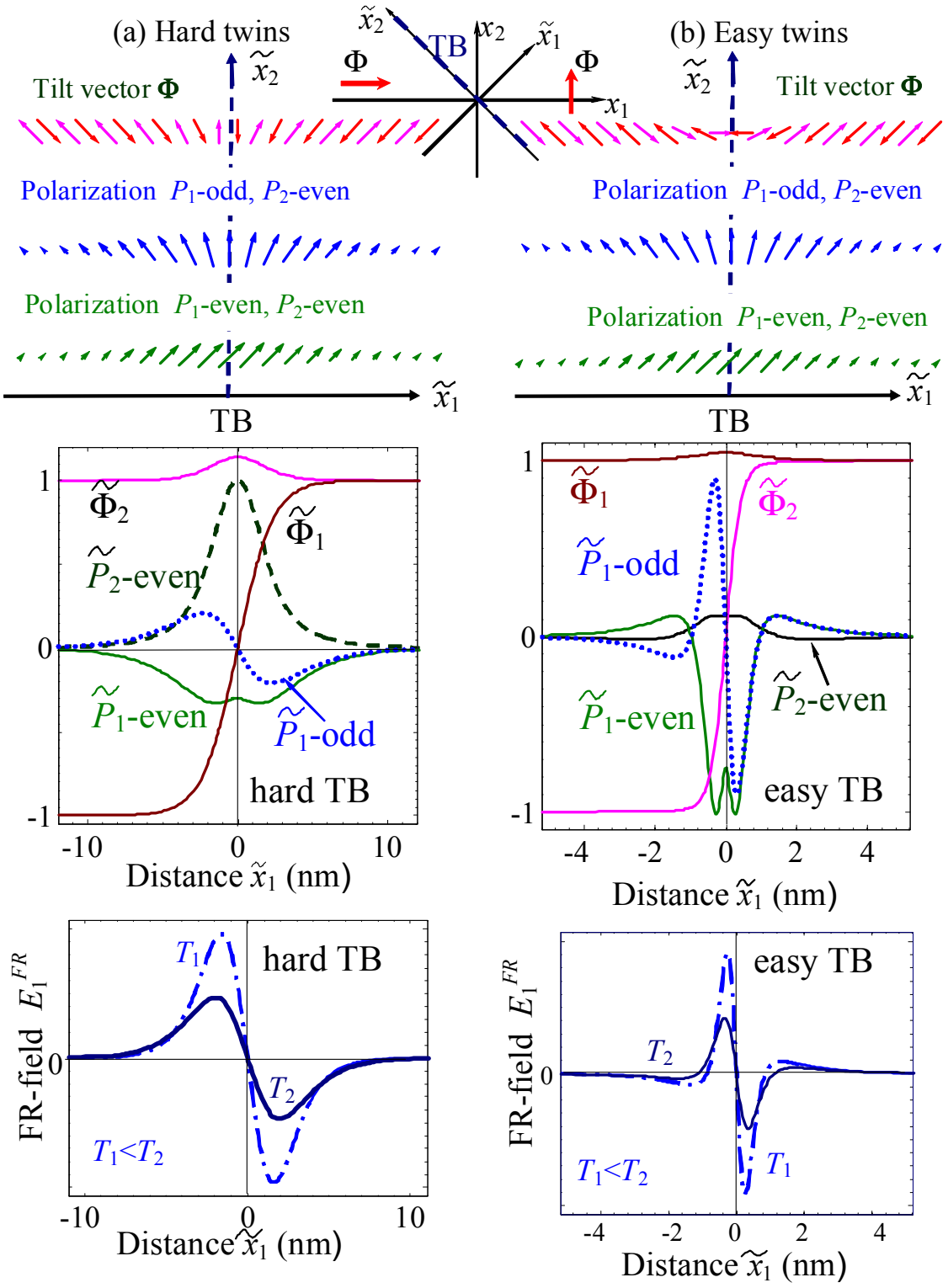

Figure 4. Schematics of 90-degree TB: rotation vector **Φ** is parallel (a) or perpendicular (b) to the domain wall plane in the immediate vicinity of the wall plane. Polarization appears inside the twins. TB plane $\widetilde{x}=0$ (denoted as TB-plane) is in the centre. Flexo-roto fields are shown at the bottom plots.

Temperature dependences of the maximal and average spontaneous polarization values calculated inside hard TB are shown in **Figs. 5a-b**. Under the absence of the flexoelectric field spontaneous polarization and pyroelectric coefficient are zero at temperatures higher than the effective Curie temperature T_C^{TB} (see curves 1, 2 calculated at $F_{ij} \equiv 0$ and $\eta_{ij} \neq 0$). The flexo-roto effect rather weakly influences on the polarization component $\widetilde{P}_2$. For the case $F_{ij} \neq 0$ the component $\widetilde{P}_1 \sim E_1^{FR}$ appears below T_S, firstly quasi-linearly increases with temperature decrease, then non-linearly increases, then has a pronounced jump at T_C^{TB} and then saturates at low temperatures $T << T_q$. The jump at T_C^{TB} originates from the appearance of reversible ferroelectric polarization component $\widetilde{P}_2$ below T_C^{TB} The maximal values of polarization are very close for odd and even types of solutions in the dielectric limit. Allowing for the flexo-roto-effect contribution we obtained $\widetilde{P}_2 \sim 2$ μC/cm^2 and $\widetilde{P}_1 \sim 0.02$ μC/cm^2 below T_C^{TB}. Without the flexo-roto-effect $\widetilde{P}_2$ is still ~2 μC/cm^2 at low temperatures, but $\widetilde{P}_1 < 0.005$ μC/cm^2.

Temperature dependences of the maximal and average pyroelectric coefficients $\widetilde{\Pi}_2$ and $\widetilde{\Pi}_1$ of hard TB are shown in **Figs. 5c-d**. Pyroelectric coefficients appear below T_S only at nonzero flexoelectric coefficient $F_{ij} \neq 0$. Pyroelectric coefficient $\widetilde{\Pi}_1$ has two maximums: a smooth maximum at the polarization inflection point ~80 K and the sharp maximum at T_C^{TB} originated from $\widetilde{P}_2$ appearance, since $\widetilde{P}_2$ enhances $\widetilde{P}_1$ via the biquadratic coupling term $\widetilde{\eta}_{66}\widetilde{\Phi}_2\widetilde{\Phi}_1\widetilde{P}_2$ in corresponding equation of state. Pyroelectric coefficient $\widetilde{\Pi}_2$ has a single sharp maximum at T_C^{TB} corresponding to the second order ferroelectric phase transition (appearance of the ferroelectric polarization $\widetilde{P}_2$). Pyroelectric coefficients monotonically decrease below T_C^{TB} with the temperatures decrease due to the spontaneous polarization components saturation at temperatures $T << T_q$.

Allowing for the flexo-roto-effect contribution we calculated pyroelectric coefficients of the even-type distributions averaged across hard TB: $\left\langle \widetilde{\Pi}_2 \right\rangle \sim 2\times10^{-3}$ C/m^{2}K and $\left\langle \widetilde{\Pi}_1 \right\rangle \sim 2\times10^{-6}$ C/m^{2}K around T_C^{TB}. The values of $\left\langle \widetilde{\Pi}_2 \right\rangle$ are well above detectable limit, $\left\langle \widetilde{\Pi}_1 \right\rangle$ is within the limit [44]. The halfwidth of hard TB is not less than 3 nm at 0 K and 5 nm at 90 K (see **Fig.S2, Suppl.Mat. [43]**). We hope that PyroSPM [39] supplied with sharp tips of sizes 5-10 nm could detect pyroelectric response

averaged over the TBs width and thus our results could provide motivation to apply this method to study of $SrTiO_3$ domain walls.

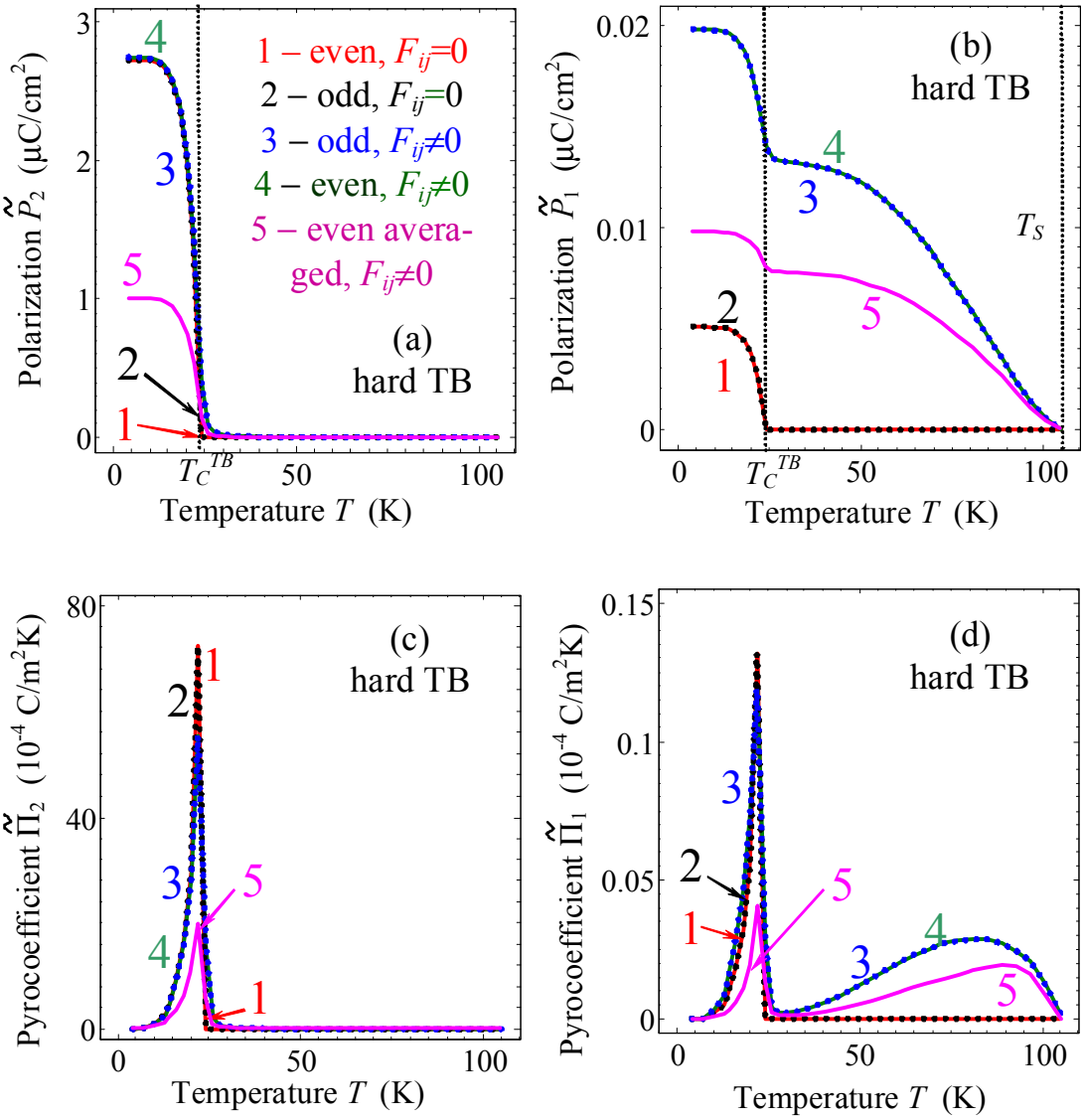

Figure 5. Temperature dependences of spontaneous polarization components $\tilde{P}_2$ and $\tilde{P}_1$ maximal values (a,b) and corresponding pyroelectric coefficient components $\tilde{\Pi}_2$ and $\tilde{\Pi}_1$ (c,d) calculated for hard TB in $SrTiO_3$ without free carriers. Temperature dependences are calculated for nonzero flexoelectric effect $F_{ij} \neq 0$ and biquadratic coupling $\eta_{ij} \neq 0$ (curves 3, 4, 5) and for the case of nonzero biquadratic coupling $\eta_{ij} \neq 0$ and zero flexoelectric effect $F_{ij} \equiv 0$ (curves 1, 2). Curves 1-4 are maximal values, curves 5 – are the even even-type distributions *averaged across TB width,* which temperature dependence is shown in **Fig.S2, Suppl. Mat [43]**. Curves 1-5 style and colour coding for

plots (a-d) are the same and described in the legend to plot (a). Material parameters are listed in the **Table 1.**

To summarize the section 3, let us underline that pyroelectric response and polarization across TB and APB in $SrTiO_3$ originate from the flexo-roto effect in the temperature range $T_C^{APB,TB} < T < T_S$ and should exist in other ferroelastics incipient-ferroelectrics like in $CaTiO_3$ and $EuTiO_3$.

Summary

In summary, we report a new mechanism, namely through the coupling of flexoelectric and rotostriction effects, that can give rise to the appearance of a significant improper spontaneous polarization and pyroelectricity across a structural antiphase boundary and twins, and by extension across interfaces in otherwise non-ferroelectric perovskites such as $CaTiO_3$, $SrTiO_3$, and $EuTiO_3$. In $SrTiO_3$, we show that this mechanism leads to a spontaneous polarization and pyroelectricity with an onset at a higher temperature than previously predicted through other coupling mechanisms (**Table 2**).

Table 2

Polarization and pyro-coefficients	**Hard 180-degree tilt APB and Hard 90-degree tilt TB**	**Easy 180-degree tilt APB and Easy 90-degree tilt TB**
Polarization component $P_{\parallel}$ **parallel** to the domain wall plane	Ferroelectric hysteresis loop $P_{\parallel}(E_{\parallel})$ exists at $0<T<T_C^*$	Identically zero for easy APB Negligibly small for easy TB
	Second order phase transition to ferroelectric phase occurs at $T=T_C^*$	
	Hysteresis loop is absent at $T_C^*<T<T_S$. At these temperatures the amplitude $P_{\parallel}$ is proportional to $\eta\Phi_{\perp}\Phi_{\parallel}P_{\perp}$	
Polarization component $P_{\perp}$ **perpendicular** to the domain wall plane	Amplitude $P_{\perp}$ is proportional to the local flexoelectric field E^{FR} and $\eta\Phi_{\perp}\Phi_{\parallel}P_{\parallel}$ at $0<T<T_S$. Ferroelectricity and hysteresis loop for $P_{\perp}(E_{\perp})$ is absent due to the strong depolarization field	Amplitude $P_{\perp}$ is proportional to the local flexoelectric field E^{FR} at $0<T<T_S$. Ferroelectricity and hysteresis loop for $P_{\perp}$ is absent due to the strong depolarization field
Pyroelectric	Increases with T increase at $0<T<T_C^*$	Identically zero for easy APB

response **parallel** component $\Pi_{\parallel} = dP_{\parallel}/dT$	Sharp maximum occurs at $T=T_C^*$ and then response decreases with T increase at $T_C^*<T<T_S$	Negligibly small for easy TB
Pyroelectric response **perpendicular** component $\Pi_{\perp} = dP_{\perp}/dT$	Increases with T increase at $0<T<T_C^*$	$\Pi_{\perp}$ is nonzero in the temperature range $0<T<T_S$, but vanishes at low temperatures $T\rightarrow 0$ and tends to zero at $T\rightarrow T_S$
	Sharp maximum occurs at $T=T_C^*$, since in the vicinity of T_C^* $\Pi_{\parallel} \sim \Pi_{\perp}$ via the coupling term $\eta\Phi_{\perp}\Phi_{\parallel}P_{\parallel}$	
	Smooth maximum exists at polarization inflection point located in the range $T_C^*<T<T_S$	

*) T_C^* is effective Curie temperature that is different for APB and TB, namely $T_C^{APB} \approx 50$ K for hard APB and $T_C^{TB} \approx 25$ K for hard TB in $SrTiO_3$; T_S is the temperature of the structural phase transition.
**) FR – product of flexoelectric and rotostriction coefficients; η – biquadratic coupling coefficient.

The spontaneous polarization and average pyroelectric coefficient reaches the values ~0.1-5μC/cm^2 and ~1×10^{-3} C/m^{2}K at the $SrTiO_3$ antiphase and twin boundaries. Since the induced polarizations and pyroelectric response are well above detectable limits and since this effect is allowed at interfaces in all structures with static rotations, which are abundant in nature, it allows for an understanding of a large class of polar interfaces in nonpolar materials.

Authors gratefully acknowledge multiple discussions with Daniel Litvin, Behera K. Rakesh, and Sergei V. Kalinin; useful comments and suggestions from Alexander K. Tagantsev, and especially for his idea about interfacial pyroelectricity. National Science Foundation (DMR-0908718 and DMR-0820404) and user agreement with CNMS N UR-08-869 are acknowledged.

References

1 A. Ohtomo, D. A. Muller, J. L. Grazul, H. Y. Hwang. Nature, **419**, 378, (2002).

2 A. Ohtomo and H.Y. Hwang. Nature, **427**, 423 (2004).

3 J.W. Park, D.F. Bogorin, C. Cen, D.A. Felker, Y. Zhang, C.T. Nelson, C.W. Bark, C.M. Folkman, X.Q. Pan, M.S. Rzchowski, J. Levy and C.B. Eom. Nature Communications, **1**, 94 (2010).

4 J. Seidel, L. W. Martin, Q. He, Q. Zhan, Y.-H. Chu, A. Rother, M. E. Hawkridge, P. Maksymovych, P. Yu, M. Gajek, N. Balke, S. V. Kalinin, S. Gemming, F. Wang, G. Catalan, J. F. Scott, N. A. Spaldin, J. Orenstein and R. Ramesh. Nature Materials, **8**, 229 (2009)

5 Ying-Hao Chu, Lane W. Martin, Mikel B. Holcomb, Martin Gajek, Shu-Jen Han, Qing He, Nina Balke, Chan-Ho Yang, Donkoun Lee, Wei Hu, Qian Zhan, Pei-Ling Yang, Arantxa Fraile-Rodríguez, Andreas Scholl, Shan X. Wang and R. Ramesh. Nature Materials, **7**, 478 (2008).

6 S. J. May P. J. Ryan, J. L. Robertson, J.-W. Kim, T. S. Santos, E. Karapetrova, J. L. Zarestky, X. Zhai, S. G. E. te Velthuis, J. N. Eckstein, S. D. Bader & A. Bhattacharya. Nature Materials, **8**, 892 (2009).

7 M. Stengel, D. Vanderbilt, N. A. Spaldin, Nature Materials, **8**, 392 (2009).

8 A. Vasudevarao, A. Kumar, L. Tian, J. H. Haeni, Y. L. Li, C.-J. Eklund, Q. X. Jia, R. Uecker, P. Reiche, K. M. Rabe, L. Q. Chen, D. G. Schlom, and Venkatraman Gopalan. Phys.Rev.Lett. **97**, 257602 (2006).

9 E.A. Eliseev, A.N. Morozovska, M.D. Glinchuk, B.Y. Zaulychny, V.V. Skorokhod, R. Blinc. Phys. Rev. B. 82, 085408 (2010).

10 D. A. Tenne, A. Bruchhausen, N. D. Lanzillotti-Kimura, A. Fainstein, R. S. Katiyar, A. Cantarero, A. Soukiassian, V. Vaithyanathan, J. H. Haeni, W. Tian, D. G. Schlom, K. J. Choi, D. M. Kim, C. B. Eom, H. P. Sun, X. Q. Pan, Y. L. Li, L. Q. Chen, Q. X. Jia, S. M. Nakhmanson, K. M. Rabe, X. X. Xi. Science, **313,** 1614 (2006).

11 E.V. Bursian and O.I. Zaikovskii, Fiz. Tverd. Tela **10**, 1413 (1968) [Sov. Phys. Solid State **10**, 1121 (1968)]; E.V. Bursian, O.I. Zaikovsky, and K.V. Makarov, J. Phys. Soc. Japan, **28**, Suppl. 416 (1970).

12 W. Ma and L E Cross. Appl. Phys. Lett. **79**, 4420 (2001).

13 W. Ma and L.E. Cross. Appl. Phys. Lett. **88**, 232902 (2006).

14 Craig J. Fennie and Karin M. Rabe, Phys. Rev. B, **72**, 100103(R) (2005).

15 Nicole A. Benedek and Craig J. Fennie. Phys. Rev. Lett. **106**, 107204 (2011).

16 L.Goncalves-Ferreira, Simon A. T. Redfern, Emilio Artacho, and Ekhard K. H. Salje. Phys. Rev. Lett. **101**, 097602 (2008).

17 Eric Bousquet, Matthew Dawber, Nicolas Stucki, Celine Lichtensteiger, Patrick Hermet, Stefano Gariglio, Jean-Marc Triscone and Philippe Ghosez, Nature, **452**, 732 (2008).

18 V. Gopalan and D.B. Litvin, Nature Materials 10, 376–381 (2011).

19 M. J. Haun, E. Furman, T. R. Halemane and L. E. Cross, Ferroelectrics, **99**, 55 (1989), ibidem p.13.

20 A.K. Tagantsev, E. Courtens and L. Arzel, Phys. Rev. B, **64**, 224107 (2001).

21. B. Houchmanzadeh, J. Lajzerowicz and E Salje, J. Phys.: Condens. Matter **3**, 5163 (1991)

22 M. Daraktchiev, G. Catalan, J. F. Scott, Ferroelectrics, 375, 122 (2008).

23 P. Zubko, G. Catalan, A. Buckley, P.R. L. Welche, J. F. Scott. Phys. Rev. Lett. **99**, 167601 (2007).

24 Sandra Van Aert, Stuart Turner, Rémi Delville , Dominique Schryvers, Gustaaf Van Tendeloo, Ekhard K. H. Salje. DOI: 10.1002/adma.201103717

25. M.S. Majdoub, P. Sharma, and T. Cagin, Phys. Rev. **B 77**, 125424 (2008).

26. G. Catalan, B. Noheda, J. McAneney, L. J. Sinnamon, and J. M. Gregg, Phys. Rev B **72**, 020102 (2005).

27 E.A. Eliseev, A.N. Morozovska, M.D. Glinchuk, and R. Blinc. Phys. Rev. B. **79**, 165433, (2009).

28. D. Lee, A. Yoon, S. Y. Jang, J.-G. Yoon, J.-S. Chung, M. Kim, J. F. Scott, and T. W. Noh. Phys. Rev. Lett. **107**, 057602 (2011)

29 T.A. Aslanian and A.P. Levanyuk. *Pis'ma Zh. Eksp.Teor. Fiz.,* **28**, 76 (1978). [*Soviet Phys. JETP Lett.*, **28**, 70 (1978).]

30 B. Houchmanzadeh, J. Lajzerowicz and E Salje, Phase Trans. **38,** 77 (1992).

31. P.A. Fleury and J. M. Worlock, Phys. Rev. **174**, 613 (1968).

32. J.F. Nye. Physical properties of crystals: their representation by tensors and matrices (Oxford: Clarendon Press, 1985).

33 A.K. Tagantsev, and G. Gerra, J. Appl. Phys. **100**, 051607 (2006).

34 C.H. Woo and Yue Zheng, Appl. Phys. A **91**, 59 (2007)

35 A.M. Bratkovsky, and A.P. Levanyuk, Journal of Computational and Theoretical Nanoscience, 6, 465 (2009).

36 G. Rupprecht and R.O. Bell, Phys. Rev. **135**, A748 (1964).

37 A.N. Morozovska, E.A. Eliseev, M.D. Glinchuk, Long-Qing Chen, Venkatraman Gopalan. Interfacial Polarization and Pyroelectricity in Antiferrodistortive Structures Induced by a Flexoelectric Effect and Rotostriction (v2) / http://arxiv.org/abs/1108.0019

38 A.Y. Borisevich, O.S. Ovchinnikov, Hye Jung Chang, M.P. Oxley, Pu Yu, J. Seidel, E.A. Eliseev, A.N. Morozovska, R. Ramesh, S. J. Pennycook, S.V. Kalinin. ACS Nano **4** (10), 6071 (2010).

39 J. Groten, M. Zirkl, G. Jakopic, A. Leitner, and B. Stadlober, Phys. Rev. B 82, 054112 (2010).

40 A.N. Morozovska, E.A. Eliseev, S.L. Bravina, S.V. Kalinin. Phys. Rev. **B 75**, 174109 (2007).

41. N. Tayebi, Y. Narui, R.J. Chen, C.P. Collier, K.P. Giapis, Y. Zhang. Appl. Phys. Lett. **93**, 103112 (2008).

42 S.V. Kalinin, A.N. Morozovska, L.Q. Chen, B.J Rodriguez, Rep. Prog. Phys. **73**, 056502 (2010).

43 See Supplemental Material at [URL will be inserted by publisher] for equations describing APBs, TBs, their energies and wall halfwidth temperature dependences

44 S.B. Lang. Physics Today, **58**, № 8, 31-36 (2005).

45 Hiromoto Uwe and Tunetaro Sakudo, Phys. Rev. B **15**, 337 (1977).

46 N. A. Pertsev, A. K. Tagantsev, and N. Setter, Phys. Rev. B **61**, R825 (2000).

47 W. Cao and R. Barsch, Phys. Rev. B, **41**, 4334 (1990)

48 G.A. Smolenskii, V.A. Bokov, V.A. Isupov, N.N Krainik, R.E. Pasynkov, A.I. Sokolov, *Ferroelectrics and Related Materials* (Gordon and Breach, New York, 1984). P. 421

49 J. Hlinka and P. Marton, Phys. Rev. B **74**, 104104 (2006).

50 R. Moos, W. Mcnesklou, K. H. Hardtl, Appl. Phys. **A 61**,389 (1995).

51 Ralf Moos and Karl Heinz Hardtl, J. Appl. Phys. **80,** 393 (1996)

52. Rakesh K. Behera, Chan-Woo Lee, Donghwa Lee, Anna N Morozovska, Susan B Sinnott, Aravind Asthagiri, Venkatraman Gopalan and Simon R Phillpot. J. Phys.: Condens. Matter. **23**, 175902 (2011).